First-principles study on the effect of Ni addition on the stability of B2 $Ti_{50}Ru_{50}$ – a supercell approach

Bongani Ngobe[1, 2,*], *Mahlaga* Molepo[2], and *Maje* Phasha[1]
[1]Advanced Materials Division, MINTEK, Randburg, South Africa
[2]School of Physics, University of the Witwatersrand, Johannesburg, South Africa

Abstract. Shape memory alloys (SMA's) are a special kind of metal alloys with unique structural properties, such as shape memory effect (SME) and pseudo-elasticity (SE) that were well-observed in TiNi alloy, which commercially trades as Nitinol. This polymorphic crystal behaviour arose from the reversible phase transition between an ordered high-temperature B2 and low-temperature martensite phase (L10/B19/B19'). Due to the high ductility of Ru, this work employed a supercell approach to track the effect of nickel addition on highly stable B2-$Ti_{50}Ru_{50}$ with the intent to stimulate SME. Thermodynamic, mechanical, electronic structure and lattice dynamic characteristics were estimated using first-principles calculations. The phonons spectra of B2 $Ti_{50}Ru_{50}$ consisted of only positive frequencies, but the addition of Ni above 18.75 at. % resulted in positive and negative frequencies, indicative of a possible martensitic transformation, which is a strong character for SME.

1 Introduction

Ti-based CsCl intermetallic compounds are formed congruently from molten metal containing near equiatomic percentage during the solidification processing [1-4]. This type of intermetallic alloys are not only known for excellent high oxidation resistance and good mechanical strength for elevated temperature applications [1, 5], but some also have the shape memory effect, a phenomenon that is governed by martensitic phase transformation between an ordered high-temperature B2 austenite phase and a lower-temperature phase, such as orthorhombic-B19 ($Ti_{50}Pd_{50}$ and $Ti_{50}Pt_{50}$) and monoclinic-B19' ($Ti_{50}Ni_{50}$) [1, 6]. Shape memory alloys are a family of alloys that, when heated or subjected to a magnetic field after deformation, can revert to their original shape by the martensitic transformation (MT), [1, 6-7].

The above-mentioned materials' behaviour was observed in $Ti_{50}Ni_{50}$, commercially trading as Nitinol® [1, 5], which was discovered by Buehler in the 1960s [8]. To date, Nitinol is used in high-tech products such as robotic arms, temperature sensing actuators and eyeglass frames because of their superior shape memory effect and super-plasticity [1, 9].

* Corresponding author: Bonganing@mintek.co.za & 2623288@students.wits.ac.za

However, Nitinol's low martensitic transformation temperature (MTT) of 373 K hinders desired technological applications at high temperatures [1, 5]. Thus PGMs-based B2 compounds such as $Ti_{50}Pt_{50}$ and $Ti_{50}Pd_{50}$ were found to surpass the MTT limitations of Nitinol, as a result, they are currently being explored as potential high-temperature shape memory alloys (HTSMAs) for applications such as in power-plants, aerospace and automotive engines [2-3, 10].

Similar to other Ti-PGM-based B2 compounds, $Ti_{50}Ru_{50}$ consists of a B2 phase that remains stable with no phase transformation observed even below room temperature [6-7].

Due to SME sensitivity to compositional change, in our previous study work, the virtual crystal approximation (VCA) was carried out to partially substitute Ru with group 10 transition metals (Ni, Pd and Pt) at a very trivial compositional step of 2.5 at.% [11- 12]. The above-mentioned approach was conducted to precisely pinpoint the critical composition at which the shape memory effect is triggered in mechanically stable B2 $Ti_{50}Ru_{50}$ compound. However, the use and reliability of the VCA approach is not yet well adopted by many researchers due to its questionable pseudo-atom principle. It was for this reason that our previous work was carried out to provide some clarity on the accuracy of the VCA approach. And, to gain some insight into some of the key underlying features behind MT and SME, the use of a matured supercell approach is deemed essential, despite its demanding computing power.

To systematically replace some of the Ru atoms with Ni atoms, this work was carried out using the supercell approach within the first-principles calculations method to predict structural properties of B2 $Ti_{50}Ru_{50-x}Ni_x$ ternary compositions that could bear SME. This composition search spanned the entire composition range (0 to 50) at Ni composition step size of 6.25 at. %.

Thus, the milestone of this work was to demonstrate the versatile use of *ab-initio* methods based on density functional theory (DFT) formalism to track the possibility of the on-set shape memory behaviour derived from the introduction of Ni to a stable B2 TiRu phase. By evaluating the thermodynamic ground state stability of the austenite (B2) phase and the corresponding mechanical, electronic and lattice dynamical properties to give an insight towards the design of new SMAs.

2 Computational method

The results reported in this work were computed using the density functional theory (DFT)-based code, the Cambridge Serial Total Energy Package (CASTEP) [13-14]. For optimal comparison, the electron exchange and correlation were described by the Perdew-Burke-Ernzerhof (PBE) functional of the generalized gradient approximation (GGA) [15-16], using the ultra-soft pseudopotentials (USPPs) [9-10]. The energy cut-off of 500 eV and the k-points of 13×13×13 were found to be sufficient to converge the total energy of our benchmark binary $Ti_{50}Ru_{50}$ and $Ti_{50}Ni_{50}$ B2 unit cells, whereas the 7×7×7 k-points were used for B2 ternary $Ti_{50}Ru_{50-x}Ni_x$ 2x2x2 supercell. The 2×2×2 supercell crystal structure used in this study work consists of 16 atoms, representing B2 $Ti_8R_{8-x}Ni_x$.

All the equilibrium B2 crystal structures were obtained through geometry optimization in the Brayden-Fletcher-Goldfarb-Shanno (BFGS) minimization scheme [17].

The convergence criterion of less than 1×10^{-5} eV/atom, the maximum residual forces of 0.03 eV/Å, the maximum residual bulk stress of 0.05GPa and the maximum atomic displacement of 1×10^{-3} Å were utilized to achieve maximum accuracy.

Fig. 1 shows a schematic representation of the crystal structures used to carry the structural and thermodynamic, mechanical, electronic and vibrational properties of all the B2 compounds reported in this work.

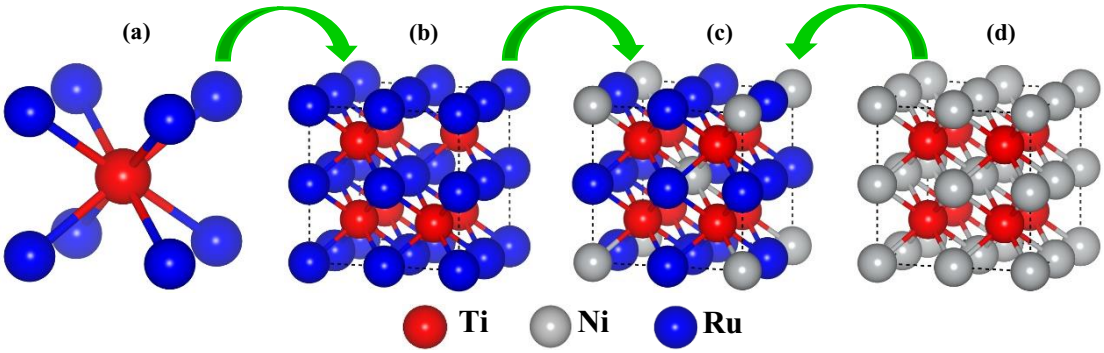

Fig. 1. Schematic representation of (a) B2 TiRu unit cell transposed to a 2×2×2 supercell crystal structures of (b) Ti_8Ru_8, (c) $Ti_8Ru_{8-x}Ni_x$ and (d) Ti_8Ni_8 intermetallic compounds, respectively.

3 Results and discussion

3.1 Structural and thermodynamic properties

Thermodynamic properties provide vital information about the behaviour of materials, such as evaluating if the desired alloy phase formation is feasible and whether it will be stable for its intended application [18]. Consequently, the enthalpy of formation (ΔH_F) as expressed in Equation 1 [19-20] is defined as the total energy difference between the compound and its constituents in proportion to the composition, which indicates the thermodynamic ability of the compound to form.

$$\Delta H_F = E_C - \sum_i x_i E_i, \quad (1)$$

where E_C represent the total energy of the intermetallic compound, and E_i represents the total energies of the participating pure elements in their stable ground-state crystal structures at x_i at. % fraction concentration. For a compound to be stable, the enthalpy (also known as the heat of formation) must have the lowest negative ($\Delta H_F<0$) value, else unstable if it has a positive value [18].

Table 1 shows the equilibrium structural and thermodynamic properties obtained in this work, such as the cell volumes, lattice parameters and enthalpies of formation. These equilibrium properties were determined from relaxed structures, where the volume and unit cell were allowed to change to attain the ground state. These reported ground state results were found to agree with those reported by other authors [9-10, 21-22], particularly the benchmark binary alloys. The data presented in Table 1 demonstrates that with an increase in Ni content, there is a corresponding decrease in the lattice parameter, leading to a subsequent reduction in the volume of the compound. This can be ascribed to the difference in atomic radii between ruthenium (1.34 Å) and nickel (1.25 Å).

Table 1. Equilibrium structural and thermodynamic properties of the investigated compounds, with experimental or theoretical data in parenthesis for comparison.

B2 compounds	**Structural properties**		
	Lattice parameters, a (Å)	Enthalpies of formation, ΔH_F (eV/atom)	Volume (Å^3)
$Ti_{50}Ru_{50}$	3.08 (3.07)	-0.76 (-0.77)	233.75
$Ti_{50}Ru_{43.75}Ni_{6.25}$	3.08	-0.70	232.26
$Ti_{50}Ru_{37.5}Ni_{12.5}$	3.07	-0.65	230.61
$Ti_{50}Ru_{31.25}Ni_{18.75}$	3.06	-0.60	228.95
$Ti_{50}Ru_{25}Ni_{25}$	3.05	-0.56	226.87
$Ti_{50}Ru_{18.75}Ni_{31.25}$	3.04	-0.51	225.13
$Ti_{50}Ru_{12.5}Ni_{37.5}$	3.04	-0.48	223.15
$Ti_{50}Ru_{6.25}Ni_{43.75}$	3.04	-0.44	221.03
$Ti_{50}Ni_{50}$	3.02 (3.02)	-0.41(-0.36)	219.01

The enthalpies of formation calculated in this study are presented in Table 1, including the existing experimental or theoretical data for binaries in parenthesis. All of the alloy compositions under investigation have negative ($\Delta H_F<0$) formation enthalpies. When comparing the thermodynamic stability of the investigated alloy compositions to that of the most stable benchmark compound, $Ti_{50}Ru_{50}$ (-0.76 eV/atom), it is evident that the introduction of Ni led to a decrease in thermodynamic stability. The findings of this study agree with those of other researchers, particularly those who have reported on binary compounds [9–10, 21–22].

3.2 Electronic properties

Fig. 2 shows the obtained total density of states (TDOS) of all the investigated binary and ternary compounds. The TDOS is used to predict electronic stability by observing the behaviour of states near the Fermi level ($E-E_F=0$) with respect to the pseudogap. The density of states also provides insights into phase stability.

An ordered intermetallic phase is stable at low temperatures if E_F cuts the pseudogap at the centre. However, if the ordered phase forms but is only stable at high temperature then E_F shifts and cuts on the shoulder of either of the DOS peaks, indicating instability of the phase at 0 K. Thus, low and high DOS at E_F is considered to be related to the structural stability and instability, respectively [23]. Consequently, those systems with higher energy at the anti-bonding region (above E_F) will undergo the martensitic transformation and hence often exhibit the shape memory effect [2, 24].

All the B2 compounds reported in this study work were found to be non-zero at the Fermi level indicating they all consist of metallic bonds. Further shown in Fig. 2 for our benchmark parent alloy $Ti_{50}Ru_{50}$, the E_F was found to cut its TDOS at the centre of the pseudogap, indicating that B2 $Ti_{50}Ru_{50}$ will remain stable with no prospect of phase transition.

While E_F of Nitinol cuts at the shoulder of the deep valley indicating instability with a high prospect of undergoing martensitic phase transition. This observation is in good agreement with other work reported in the literature [25].

Fig. 2 further shows that replacing some Ru atoms with Ni atoms has a compounding effect on the resultant ternary compounds, with its E_F shifting towards the anti-bonding region. The above is an authentication that systematically alloying stable $Ti_{50}Ru_{50}$ with Ni atoms was found to have induced martensitic phase transformation on a stable B2 TiRu system.

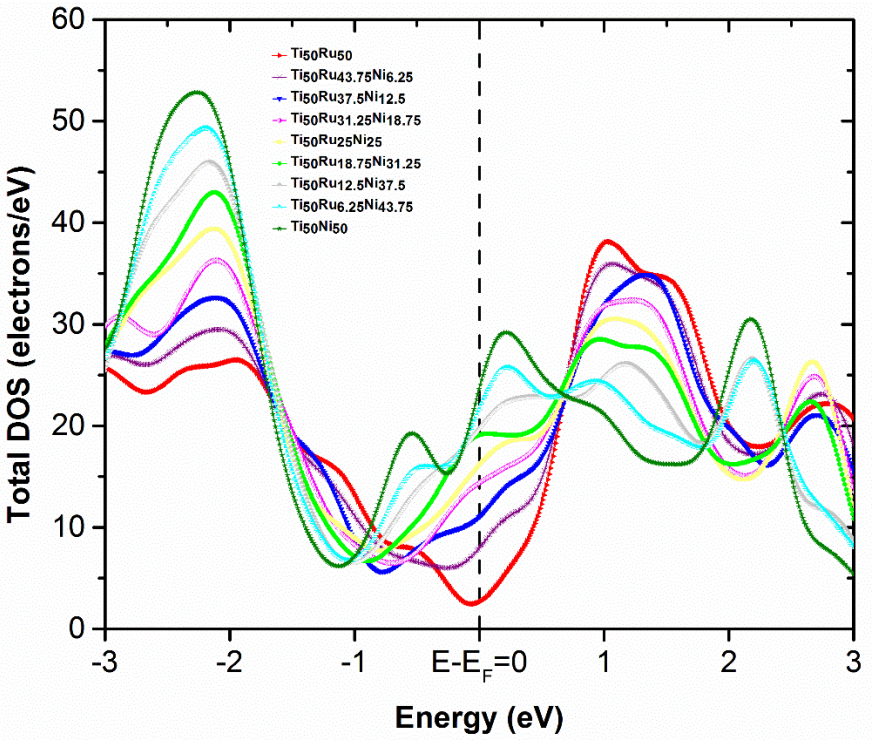

Fig. 2. Total density of states (TDOS) of the investigated B2 compounds.

3.3 Elastic properties and mechanical stability

Elastic properties provide fundamental information about the bonding character between adjacent atomic planes, the anisotropic character of bonding, the mechanical stability and the rigidness of solid materials [9, 26-27]

The mechanical stability of a crystal can be determined from the computed elastic constants (C_{ij}) [9]. B2 compounds consist of a cubic system with only three independent elastic constants, namely, C_{11}, C_{12} and C_{44}.

On the other hand, Born-Huang's lattice dynamical theory [22, 28-29] states that the cubic mechanical stability criterion can be endorsed by satisfying all the impartialities given in Equation 2.

$$C_{11} > 0, C_{44} > 0, C_{11} - C_{12} > 0, C_{11} + 2C_{12} > 0 \quad (2)$$

In addition to indicating mechanical stability, a shear elastic coefficient (C') determined using the expression in equation 2, may also be used for assessing the compound's prospect to undergo phase transition

$$C' = \left(\frac{C_{11}-C_{12}}{2}\right) \quad (3)$$

The mechanical stability of a crystal decreases when approaching the phase transition [30-31], this is at the point where C' becomes smaller than the trigonal shear constant (C_{44}) which represents the crystal's resistance against shearing. Fig. 3 presents the elastic constants of the investigated B2 compositions, and all compounds found to comply with the Born-Huang's theory for cubic crystals.

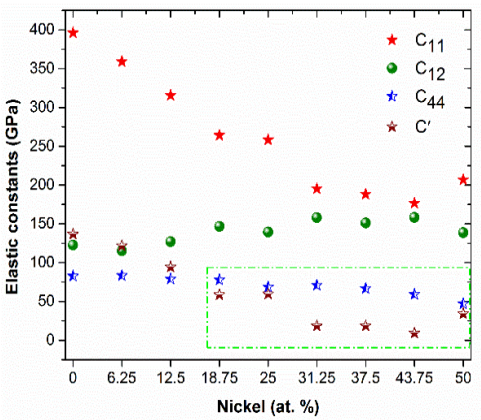

Fig. 3. The elastic constants of the investigated B2 compounds

In contrast to the stable B2 $Ti_{50}Ru_{50}$, Fig. 3 further shows that $Ti_{50}Ru_{50-x}Ni_x$ compositions with Ni composition above 12.5 at. % have C_{44} values that are higher than the corresponding C' values, leading to an elastic anisotropy factor (A^Z) greater than 1. As more Ni atoms are added, C' gets closer to 0, increasing the likeliness of undergoing a phase transition, comparable to what has been observed on Nitinol.

Elastic moduli such as the Bulk modulus (B), Shear modulus (G), Young's modulus (E), Poisson's ratio (v) as well as the Zener elastic anisotropy (A^Z) are used to determine the mechanical properties of structural materials [27]. They can be obtained from the three independent elastic constants C_{ij} using the Voigt-Reuss-Hill approximation [29] with the following set of expressions given in Equation 4 for cubic crystals.

$$B_V = B_R = \frac{1}{3}(C_{11} + 2C_{12}),\ G_V = \frac{1}{5}(C_{11} - C_{12} + 3C_{44}),\ G_R = \frac{5(C_{11}-C_{12})C_{44}}{4C_{44}+3(C_{11}-C_{12})} \quad (4)$$

Subsequently, B and G can be deduced as average values given by $B = (B_V + B_R)/2$ and $G = (G_V + G_R)/2$, while E and v can be computed from $E = 9GB/(G + 3B)$ and $v = (3B - E)/6B$ respectively.

The bulk and shear modulus respectively provide the material's resistance to volume change and shear resistance against external forces [32].

Young's modulus gives features of materials' stiffness, higher E consists of ionic/covalent bonds whereas lower E signifies metallic bonds that are easy to deform [32-33]. Another important aspect of mechanical stability is hardness, which measures solid materials' resistance to plastic or permanent deformation [34]. First-principles estimate crystals' hardness from an empirical hardness [34], using the expression given in Equation 5.

$$H_V = 0.92\left(G/B\right)^{1.137} \times G^{0.708} \quad (5)$$

The relationship between the interatomic bonding and the physical properties can be determined by using Pugh's ratio (B/G) and v. Pugh's ratio has a threshold of 1.75, such that if B/G>1.75 signifies ductility, and if less than 1.75 signifies brittle [35]. Poisson's ratio has a threshold of 1/3, if v is less than 1/3 the alloy is made up of ionic or covalent bonds, and if v is larger than 1/3 the bonds are metallic which are ductile in nature [33-36].

Although the Zener anisotropy was reported to quantify the instability of the alloy [31], it seems more appropriate to associate this property with the flexibility of the material. Hence A^Z for pure metals ranges between 1 and 3, while that of copper is 3.21 and for SMA it often reaches higher values [31].

Fig. 4 (a) – (b) presents all the moduli calculated in this study. In Fig. 4 (a), our stable Ti_8Ru_8 was found to be rigid with larger *B, G* and *E* indicating strong mechanical stability. However, as Ru atoms are substituted by atoms of malleable Ni, an increase in ductility becomes evident and more pronounced at Ni composition close to 25 at. % and above. It is known that hardness can also be characterized as the ability of a material to resist both elastic and plastic deformation [37]. Thus, as shown in Fig. 4 (a), an opposite linear trend is observed on the predicted hardness (*H*), *G*, *E* and *B* against the increase in Ni composition showing softening.

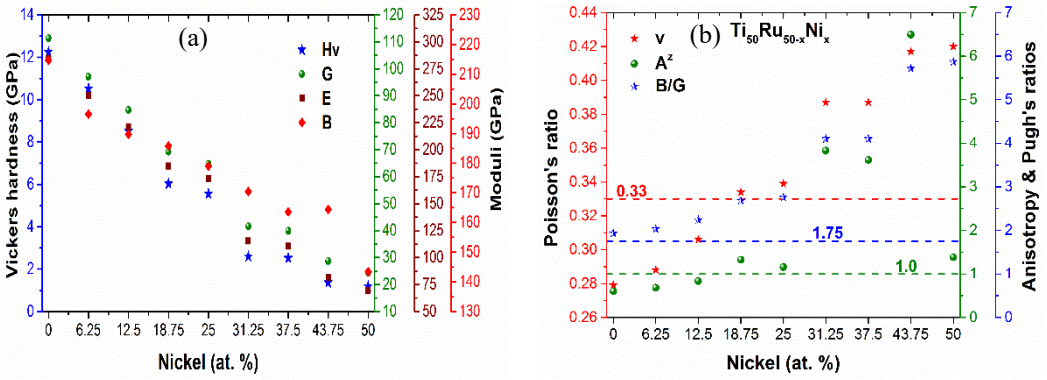

Fig. 4. The (a) Modulus of elasticity and (b) Pugh's, Poisson's as well as the Zener anisotropy ratios of the investigated compounds

Fig. 4 (b) presents Pugh's, Poisson's and anisotropic ratios of the investigated compositions. It follows from Fig. 4 (b) shows that *v* for stable B2 $Ti_{50}Ru_{50}$ and ternaries with Ni composition less than 18.75 at. % is found to be less than 1/3 indicating their ionic/covalent bonding. While for 18.75 at. % and above, *v* was found larger than 1/3 indicating metallic bonding which is ductile.

However, this ductile and bonding observation seems to be in contrast with Pugh's ratio. It can be seen furthermore in Fig. 4 (b) that in all the investigated compounds, *B/G* was found to be greater than 1.75, predicting that they are all ductile in spite of the fact that B2 $Ti_{50}Ru_{50}$ is known to be very brittle [11, 38], and its Pugh's ratio should be less than 1.75.

It appears Pugh's ratio is more appropriate to predict the ductility of FCC crystals than for BCC crystals whereas Poisson's ratio is consistent for both cubic crystal types. The work conducted by Phasha et al. provides further evidence of the aforementioned observations, where the Pugh's ratio of a well-known ductile B2 MgLi was reported to be less than 1.51, signifying brittleness [39-40].

In an attempt to remedy such contrast, the anisotropic ratio of the investigated compounds was calculated in this study. As observed in Fig. 4 (b), the A^Z was found to be less than 1, corresponding with the Poisson's ratio values of less than 1/3, for B2 $Ti_{50}Ru_{50}$ as well as for compositions with Ni content at 12.5 at.% and less. Current results confirm that stable B2 $Ti_{50}Ru_{50}$ is indeed brittle, and the same applies for $Ti_{50}Ru_{50-x}Ni_x$ with Ni composition ≤ 12.5 at. %.

3.4 Lattice dynamic properties

Phonons are induced by the collective vibration of ions within a crystal. Information derived from phonons is very useful to account for a variety of properties and behaviour of crystalline materials, such as thermal properties, mechanical properties, phase transition, and superconductivity [41].

Phonons are instrumental features in evaluating alloys that are deemed to have shape memory effects. Thus, this study further investigated the effect of Ni alloying on lattice dynamic properties using computed phonon dispersion curves.

A compound is considered stable at 0 K if there are no soft modes along high symmetry directions in the Brillouin zone (BZ). In addition, the presence of soft modes or negative frequencies indicates the lattice, an indication of the likelihood to undergo a phase transition [30, 41].

Fig. 5 graphically presents sets of phonon dispersion spectrums that were computed at 0 K for the investigated binary and ternary B2 compounds. The obtained results show that the phonon spectra for ordered pristine B2 $Ti_{50}Ru_{50}$ and the ternary compositions with Ni content $\leq$ 18.75 at. % were found to consist of only the positive vibrational frequencies [10, 30], denoted by the red oscillating bands. This is an indication that these B2 compounds do not undergo any phase transformation even at 0 K, a further confirmation that B2 $Ti_{50}Ru_{50}$ remains stable down to room temperature with no phase transition.

In contrast, the substitution of brittle Ru atoms with ductile Ni atoms in larger quantities demonstrated a compounding effect on the vibrational behaviour of the stable B2 $Ti_{50}Ru_{50}$ phase. This is shown in Fig. 5 where the ternary compounds with Ni composition above 18.75 at. % (denoted by the blue oscillating bands) has triggered negative vibrational frequencies with features that closely resemble those of Nitinol, more especially at much higher Ni content, signalling a possible martensitic transformation.

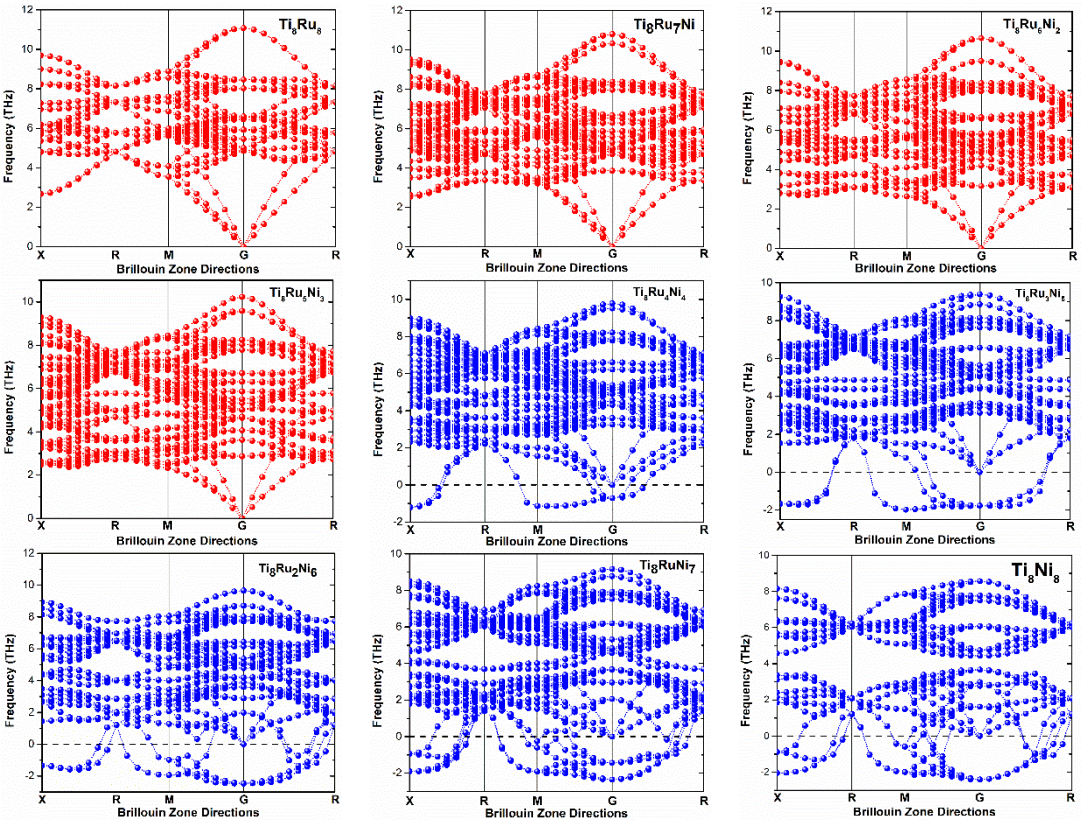

Fig. 5. Phonon dispersion curves of the benchmark B2 binary and $Ti_{50}Ru_{50-x}Ni_x$ ternary compounds investigated

4 Conclusions

The thermodynamic, electronic, mechanical and lattice dynamic properties of the binary and ternary B2 $Ti_{50}Ru_{50-x}Ni_x$ compositions calculated using a first-principles approach are reported.

The lattice parameters and heats of formation of pristine B2 $Ti_{50}Ru_{50}$ reported in this study were found to be in good agreement with other authors' work to within an acceptable 3 % error margin, indicative of the accuracy of the computational parameters used. From the calculated enthalpies of formation, it was shown that the thermodynamic stability of the well-known stable $Ti_{50}Ru_{50}$ decreases with an increase in Ni content.

The total density of states results reveal that the addition of Ni above 12.5 at. % was found to shift the Fermi level towards the bonding state.

From the mechanical stability perspective, all compounds satisfied Born-Huang criteria ($C'>0$). At Ni compositions ≥ 18.75 at. %, C_{44} becomes greater than C', the onset of flexibility since $A^Z > 1$. The calculated Pugh's ratio of brittle B2-$Ti_{50}Ru_{50}$ was found to be 1.93, suggesting it to be ductile. As a result, this study finds the Pugh's ratio ductility threshold of 1.75 to be inappropriate for BCC crystal structures while reliable for face-centred cubic (FCC) crystals.

While the phonon spectrum for stable B2 $Ti_{50}Ru_{50}$ was found to consist of only positive frequencies, the ternary compositions with Ni content above 18.75 at. % were found to have both positive and negative frequencies, signalling a possible martensitic transformation.

This study can therefore conclude that using first-principles calculations has demonstrated that through the systematic substitution of Ru by Ni atoms, it was possible to induce martensitic phase transformation in B2 $Ti_{50}Ru_{50}$ compound, thus identifying ternary B2 compositions that could bear shape memory effect.

5 Acknowledgements

This paper is published with the permission of MINTEK and The University of the Witwatersrand. The authors would like to thank the Advanced Metals Initiative (AMI) of the Department of Science and Innovation (DSI) for financial support. MJP is grateful for financial support from the National Research Foundation (NRF) of South Africa - JSPS GRANT No: 148782. Furthermore, the gratitude is extended to the Centre for High-Performance Computing (CHPC) in Cape Town for allowing us to carry out the calculations using their remote computing resources.

References

1. A. Wadood, HEC, 1-144 (2018)
2. S.E. Kulkova, D.V. Valujsky, J. Phys. IV **11**, 53-58 (2001)
3. S.E. Kulkova, D.V. Valujsky, J. S. Kim, G. Lee, Y.M. Koo, Solid State Commun. **119**, 619-623 (2001)
4. H. Baker, ASM Handbook, 10th Edn. **3**, 1340-1378 (1992)
5. A. Wadood, Adv. Mate. Sci. Eng. **4**, 1-9 (2016)
6. H. Donkersloot, J. V. Vucht, J. Less-Common. Met. **20**, 83-91 (1970)
7. V. Khachin, Rev. Phys. Appl. **24**, 733-739 (1989)
8. W.J. Buehler, J.V. Gilfrich, R.C. Wiley, JAP **34**, 1475-1477 (1963)
9. W. Bao, D. Liu, Y. Duan, M. Peng, Philos. Mag. **99**, 1-22 (2019)
10. Z.Z. Kong, Y.H. Duan, M.J. Peng, D.Y. Qu, L.K. Bao, Physica. B: Cond. Matter. **573**, 13-21 (2019)
11. B.S. Ngobe, M.J. Phasha, I.A. Mwamba, SAJST **40**, 205-211 (2021)

12. J. Frenzel, A. Wieczorek, I. Opahle, B. Maaβ, R. Drautz, G. Eggeler, Acta Mater. **90**, 213-231 (2015)
13. M.D. Segall, J.D.L. Philip, M.J. Probert, C.J. Pickard, P.J. Hasnip, S.J. Clark, M.C. Payne, J. Phys. D: Condens. Matter. **14**, 2717-2744 (2002)
14. P.E. Blöchl, Phys. Rev. B **50**, 17953-17978 (1994)
15. J.P. Perdew, Y. Wang, Phys. Rev. B **45**, 13244-13249 (1992)
16. S. Plimpton, J. Comp. Phys. **117**, 1-19 (1995)
17. T. Fischer, J. Almlof, J. Phys. Chem. **96**, 9768-9774 (1992)
18. J. Yang, J.H. Huang, Z. Ye, D.Y. Fan, S.H. Chen, Y. Zhao, Ceram Int. **43**, 7751-7761 (2017)
19. R. Jaradat, M. Abu-Jafar, I. Abdelraziq, A. Mousa, T. Ouahrani, R. Khenata, AIP Adv. **8**, 1-20 (2018)
20. W.W. Xing, X. Q. Chen, D.Z. Li, L.Y. Li, C.L. Fu, Intermetallics. **28**, 16-24 (2012)
21. T. Philip, P. Beck, Trans. AIME. **209**, 1269-1271 (1957)
22. J. Jung, G. Ghosh, G. Olson, Acta Mater. **51**, 6341-6357 (2003)
23. J.M. Zhang, G.Y. Guo, J. Phys. Condens. Matter. **7**, 6001-6017 (1995)
24. P. Ravindran, R. Asokamani, Bull. Mater. Sci. **20**, 613-622 (1997)
25. R. John, H. Ruben, Mater Sci. Appl. **2**, 1355-1366 (2011)
26. S.K. Khandy, D.C. Gupta, RSC Adv. **6**, 48009-48015 (2016)
27. S. Liu, C. Tang, Y. Zhan, Met. And Mat. Trans. **47A**, 1451-1459 (2016)
28. M. Wagner, W. Windl, Acta Mat. **56**, 6232-6245 (2008)
29. O. Gomisa, F.J. Manjónb, P. Rodríguez-Hernándezc, A. Muñozc, J.Phys. Chem. Solid. **124**, 111-120 (2019)
30. L. Si, Z.-Y. Jiang, B. Zhou, W.-Z. Chen, Phys. **B 407**, 347-351 (2012)
31. P. Sedlák, M. Janovská, L. Bodnárová, O. Heczko, H. Seiner, Metals **10**, 1-13 (2020)
32. J. Zhang, C. Mao, C.G. Long, J. Chen, K. Tang, M.J Zhang, P. Peng, JMA **3**, 127-133 (2015)
33. E. Jain, G. Pagare, S.S. Chouhan, S.P. Sanyal, Intermetallics **54**, 79-85 (2014)
34. J. Yun-Fei, Y. Xiang-Xi, L. Jing-Tian, Z. Wen-Xian, Z. Jun, N. Xi-Jing, Chinese Phys. Lett. **27**, 076201- 076203 (2010)
35. L. Liu, X. Wu, R. Wang, X. Nie, Y. He, X. Zou, Cryst. **7**, 1-10 (2017)
36. D. Chen, Z. Chen, Y. Wu, M. Wang, N. Ma, H. Wang, Comp. Mater. Sci. **91**, 165-172 (2014)
37. J.H. García, J.C. Hernández, J. Mat. Sci. Eng. **3**, 31-34 (2016)
38. M. Tsuji, H. Hosoda, K. Wakashima, Y. Yamabe-Mitarai, MRS Symp. Proc. **753**, BB5.52.1-BB5.52.6 (2023)
39. M.J. Phasha, P.E. Ngoepe, H.R. Chauke, D.G. Pettifor, D. Nguyen-Mann, Intermetallics. **13**, 2083-2089 (2010)
40. M. Phasha, M. Mulaudzi, H. Moller, SAJIE. **33**, 339-346 (2022)
41. A. Togo, I. Tanaka, Scri. Mater. **108**, 1-5 (2015)